Measurements and Retrievals From a New 183-GHz Water-Vapor Radiometer in the Arctic

Maria P. Cadeddu, James C. Liljegren, and Andrew L. Pazmany, *Member, IEEE*

Abstract—**A new G-band (183.31-GHz) water-vapor radiometer, developed and built by ProSensing Inc., was deployed in Barrow, AK, in April 2005. The radiometer is part of a suite of instruments maintained by the Atmospheric Radiation Measurement program. The instrument measures brightness temperatures from four double-sideband channels centered at ±1, ±3, ±7, and ±14 GHz from the 183.31-GHz water-vapor line. Atmospheric emission in this spectral region is primarily due to water vapor, with some influence from liquid water. In this paper, data collected in November 2005, December 2005, and January 2006 are analyzed. Measurements are compared with simulations obtained by using a radiative transfer model. We show that the measurements agree well with model simulations. Precipitable water vapor (PWV) and liquid water path (LWP) are retrieved with a nonlinear physical algorithm, and results are compared with those from the colocated dual-channel microwave radiometer and radiosondes. Retrieval errors are estimated to be below 5% for PWV and of the order of 0.006 mm for LWP.**

Index Terms—**Microwave radiometry, remote sensing, water-vapor retrieval, 183 GHz.**

I. Introduction

THE G-BAND (183.31 GHz) water-vapor radiometer (GVR) is part of a suite of instruments deployed by the Atmospheric Radiation Measurement (ARM) Program [1] to improve observations of low amounts of precipitable water vapor (PWV $<$ 5 mm) and low amounts of liquid water path (LWP $<$ 50 g/m^2). Water vapor, as one of the most variable atmospheric constituents, is a critical element in the analysis of local weather patterns, as well as in the validation of global-climate models. Accurate water-vapor measurements are essential in assessing the performance of clear-sky radiative-flux models. Microwave radiometry is also an established method to retrieve accurate LWP, which is necessary to the study of the role of clouds in the earth-radiation balance.

PWV retrieval errors achieved with traditional linear statistical retrievals from microwave measurements are approximately 0.4 mm, and LWP retrieval errors are around 0.02 mm (or 20 g/m^2); however, as shown in [2], a large percentage of clouds have LWP of less than 100 g/m^2. Traditional ground-based measurements employ two or more channels located in the spectral region of water-vapor absorption near 22 GHz and one channel in the window region near 30 GHz where liquid-water absorption dominates during cloudy conditions. The ARM Program has been operating a two-channel microwave radiometer (MWR) with frequencies at 23.8 and 31.4 GHz for several years. During the cold Arctic winter, the amount of PWV is often less than 3 mm, and clouds with LWP of less than 50 g/m^2 are common. In these conditions, the dual-channel MWR is operating at the limit of its capabilities with a very low signal-to-noise ratio. Several authors [2]–[4] have analyzed the origin of uncertainties in MWR retrieval. In addition to calibration issues and the effect of measurement noise, uncertainty in the liquid-water retrieval can be attributed to the modeling of the dry-opacity term and to the cloud-liquid-absorption coefficient. One result of these uncertainties is that the MWR can retrieve LWP significantly higher or lower than zero when the sky is clear (i.e., when there are no liquid clouds).

Because of its increased sensitivity to water vapor, the 183.31-GHz absorption line can help improve water-vapor retrievals during the dry Arctic winter. However, the dependence of brightness temperatures on PWV and liquid water is linear only in a limited range for this frequency, and a nonlinear retrieval algorithm is needed. Additionally, the radiometer response saturates at a PWV of approximately 5 mm [5] for the most sensitive channels. The absorption line centered at 183.31 GHz has been extensively used from satellites [6] and aircraft [7], however, very few measurements [5], [8], [9] have been reported from the ground. The GVR has been operating in Barrow, AK, since April 2005, and is the first ground-based radiometer, operating at 183.31 GHz, permanently deployed at an Arctic location for the purpose of improving PWV and LWP retrievals.

The GVR was developed by ProSensing under a Department of Energy Small Business Innovation Research grant [10]. The objective of the first year of operation at the North Slope of Alaska (NSA) site at Barrow was to evaluate its performance. The purpose of this paper is to analyze the data from the GVR and to assess the instrument's capability of supplementing the MWR retrievals in very dry conditions. This paper is organized as follows. In Section II, a brief description of the instrument is given. In Sections III and IV, measured brightness temperatures are compared to model computations and the effect of uncertainties in radiosonde (RS) soundings is assessed. In Section V, the sensitivity of measured brightness temperatures

Manuscript received May 24, 2006; revised August 30, 2006. This work was supported by the Climate Change Research Division, U.S. Department of Energy, Office of Science, Office of Biological and Environmental Research, under Contract W-31-109-Eng-38, as part of the ARM Program. The Argonne National Laboratory is managed by the University of Chicago for the U.S. Department of Energy.

M. P. Cadeddu and J. C. Liljegren are with the Argonne National Laboratory, Argonne, IL 60439 USA (e-mail: mcadeddu@anl.gov; jcliljegren@anl.gov).

A. L. Pazmany is with ProSensing, Inc., Amherst, MA 01002 USA (e-mail: pazmany@prosensing.com).

Color versions of one or more of the figures in this paper are available online at http://ieeexplore.ieee.org.

Digital Object Identifier 10.1109/TGRS.2006.888970

to water vapor and cloud-liquid water are assessed. The retrieval algorithm is described in Section VI, and in Section VII, PWV and LWP retrievals are discussed, retrieval errors are theoretically quantified, and their dependence on the amount of PWV is shown. Our data set has also provided us with the opportunity to carry out an extensive comparison with retrievals from the MWR and Vaisala RS92 RS under a range of water-vapor conditions. Specific attention is devoted in Section VIII to the analysis of retrieved LWP under clear-sky conditions and its comparison to retrievals from the MWR. A brief summary of results is given in Section IX.

II. Instrument

The GVR [10] measures brightness temperatures from four double-sideband channels centered at ±1, ±3, ±7, and ±14 GHz around the 183.31-GHz water-vapor line. Atmospheric emission in this spectral region is primarily due to water vapor, with some influence from liquid water. The 183.31 ± 14-GHz channel is particularly sensitive to the presence of liquid water. Bandwidths for the four channels are 0.5, 1.0, 1.4, and 2.0 GHz, respectively. The GVR started collecting data successfully immediately after deployment. On the first day of collection, it was found that a radar operated by the U.S. Air Force in the vicinity of the radiometer was causing a strong interference with all channels, in particular, the 183.31 ± 1-GHz channel. The problem caused frequent regular spikes in the data. To eliminate this effect, a filter was applied to all frequencies. The filter acts to ensure that each data point is bounded within the range of intensities defined by its neighbors. For each data point, the maximum and minimum values of the first four neighbors are determined. If the difference between the point and the maximum (or the minimum) is greater than a fixed threshold (in this case, set to 3 K), the point is replaced with the average of the four neighbors. This filter is less smoothing than a traditional median filter as it trades noise suppression for temporal resolution. For the purpose of this analysis, data collected during cold days (surface temperatures of less than 255 K) were chosen to avoid excessive noise arising from thermal instability during warm periods.

The GVR is calibrated using a warm (~293 K) and a hot (~333 K) FIRAM-160 absorber. The absorbers are tilted by about 10° to ensure a better than −60-dB reflectivity or 0.999999 emissivity. The resulting absorber-brightness temperatures are taken to be equal to their physical temperature. The warm load "floats" at the internal temperature of the GVR enclosure. The hot load, packaged in an insulated box with a Mylar window, is convection heated: Behind the absorber (opposite of the Mylar window) is a heated metal plate and a row of fans. The fans circulate the air around the load indirectly heating it. Resistance temperature detectors placed at several locations in and around the hot load indicates that the maximum temperature differences are less than 0.5 K. The average temperature reported by sensors is used as the hot-load-equivalent brightness temperature. The accuracy of the temperature sensors is approximately 0.2 K, making them the most significant source of calibration error. This is because a +0.2-K error at the 333-K hot-load temperature and a −0.2-K error at the 293-K warm-load temperature will amplify to a −2.8-K error at a 33-K sky-brightness temperature. The metal mirror of the radiometer continuously cycles between the warm load, hot load, and the sky, calibrating the instrument once every 10 s. This calibration is sufficiently frequent, as the Allan-Deviation stability of the GVR receiver was measured to be less than 0.05 K at a ΔT of 1000 s. The operational calibration of the GVR was independently verified in the spring of 2006 with an external calibration load. A larger insulated hot-load convection chamber was constructed with a higher precision temperature meter and sensors, calibrated with a NIST-traceable voltmeter and temperature probe with a 0.05-K absolute accuracy. The measured absolute error was less than 2 K in the four receiver channels over the brightness-temperature-measurement range. The brightness temperatures used in this paper are the ones originally obtained from the instrument. The revised calibration produced a slight (~1 K) increase in the brightness temperatures of the ±1 and ±3-GHz channel, slightly improving the agreement with the model. In the next section, we will apply the calibration correction to a few cases to determine the possible contribution of calibration uncertainties to the measurement.

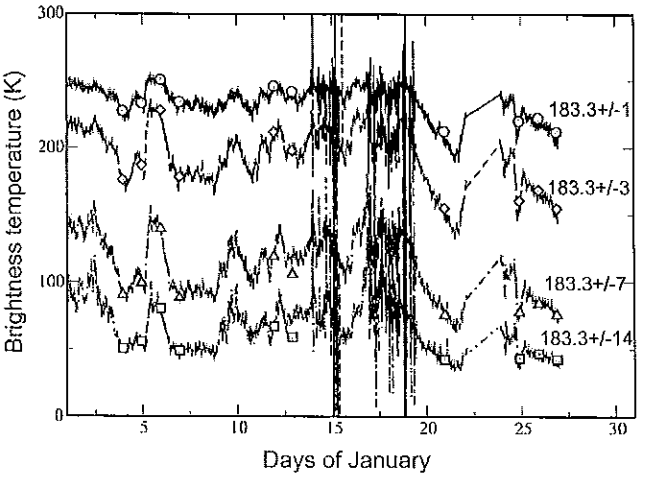

Fig. 1. Brightness temperatures measured by the GVR during the month of January. Model computations during clear-sky conditions are shown as circles, diamonds, triangles, and squares. High noise level between day 15 and 20 is due to thermal instability of the instrument.

III. Measurement-Model Comparison

The GVR has been operating continuously at the NSA site at Barrow, since April 2005. This analysis will cover data collected only during the cold winter months (November 2005–January 2006), when low-humidity conditions prevailed. A time series of data collected in January 2006 is shown in Fig. 1. Some periods of enhanced noise are visible during days 15–20. Temperature instability in the radiometer was responsible for the noise. Additional periods of enhanced noise (not shown) are present during the months of November and December.

Simulated brightness temperatures, shown in Fig. 1, were computed by using the radiative transfer code MonoRTM [11] with the HITRAN database line parameters [12] and the Clough–Kneizys–Davies 2.4 continuum [13]. For the

TABLE I
MEAN AND STANDARD DEVIATION OF MEASURED-MINUS-MODELED BRIGHTNESS TEMPERATURES AT THE NSA FROM NOVEMBER 2005 TO JANUARY 2006

Frequency (GHz)	Mean N=30 (K)	Standard deviation N=30 (K)	Mean N=24 (K)	Standard deviation N=24 (K)	Standard deviation of clear-sky measurements N=1208
183.3 ± 1	−3.57	2.24	-3.28	2.36	0.74
183.3 ± 3	−2.88	2.05	-2.92	2.22	0.91
183.3 ± 7	2.31	2.22	1.62	1.82	0.87
183.3 ± 14	0.96	3.18	-0.37	1.61	0.76

comparison monochromatic, computations at 100-MHz intervals were averaged over the full-channel bandwidth. Only RS data collected during clear conditions were used to compute brightness temperatures. The infrared temperature at 10 μm, measured by a Wintronics KT-19.85 thermometer located at the site, was used to select clear-sky cases. When the measured temperature was less than 224 K, the sky was considered free of liquid-water clouds. The clear-sky screening dramatically decreased the amount of data available for the comparison. RSs (Vaisala RS92) were launched at the NSA site once a day, five days a week. The original number of RSs available was 55 (17 in November, 18 in December, and 20 in January). Once data were screened for clouds, only 30 cases remained (11 in November, 10 in December, and 9 in January). Between the 15th and 30th of November, the radiometer experienced thermal instability. The radiometer temperature set point was decreased from 25 °C to 15 °C in several steps. Six data points of the comparison were affected by the change, and they have been identified in the following discussion. Mean and standard deviation of measured-minus-modeled brightness temperatures are displayed in Table I. In the second and third columns, the results for the 30 points are shown. In columns five and six are the results obtained if the period of thermal instability at the end of November is removed. In the fifth column is the standard deviation of a sample of 1208 points collected during clear-sky conditions at the highest rate (~8 points/min). Agreement between measurements and observations is between 2% and 3% at all frequencies. Large discrepancies between measured and modeled brightness temperatures at similar frequencies were recently reported in [5]. The improved agreement observed in this comparison can be attributed, at least in part, to improved RS measurements as discussed in the next section. Mean biases were between 0.7 and 3 K and root mean-square (rms) differences between 3 and 4 K over the range of brightness temperatures from 50–250 K. A scatter plot of measured and modeled brightness temperature is shown in Fig. 2. The larger discrepancies are observed at 183.31 ± 1 GHz, where the model overestimates the measurements by about 4 K. The overestimation has a slight dependence on the brightness temperature itself, as shown in the upper left quadrant of Fig. 2, where the slope is 0.89. The reason for the poor agreement at this frequency is not clear. Westwater *et al.* [4] showed a similar comparison of measurements and model computations using the ground-based scanning radiometer and Vaisala RS90 RSs launched at two near-by sites. Their results showed an

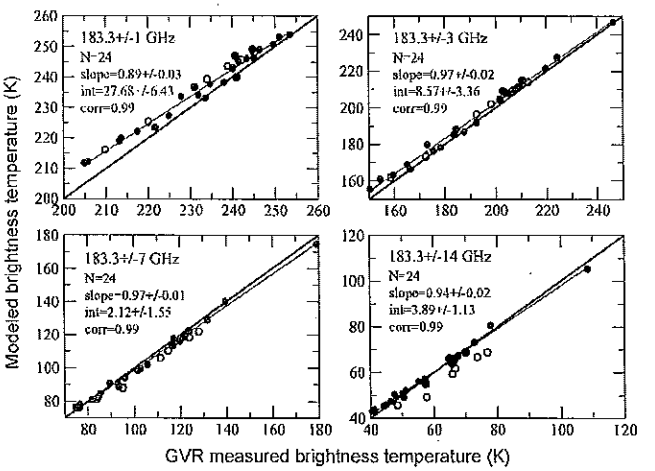

Fig. 2. Scatter plot of clear-sky measured (x axis) and modeled (y axis) brightness temperatures. Data were collected on November 2005 through January 2006 ($N = 24$). White circles are the six points during November 15–30, which are excluded from the statistics due to thermal instability of the radiometer.

rms error between measurements and model of about 3–4 K, comparable to our result, however, their agreement with the ±1-GHz channel was slightly better than in this paper. They found that differences between formulations of the water-vapor continuum contributed to differences in biases of the order of 1–2 K. The model used in this paper has a self-broadening coefficient that is about 11% smaller than the one used in [4]. This may partially explain why the agreement at this frequency is poorer than expected. In the same figure, the six points collected during the period of thermal adjustment are shown as empty circles. They show an increased scatter with respect to the other points. Near-simultaneous RS launches at Barrow produced differences of 1–1.5 K in model-calculated brightness temperatures. These differences can be used to estimate the effect of uncertainty due to RS measurements [4].

IV. EFFECT OF STRATOSPHERIC WATER VAPOR ON MODEL COMPUTATIONS

One possible source of discrepancies between measurements and model computations is the uncertainty in upper tropospheric and stratospheric soundings from RSs. This is because, as shown in [5], the weighting functions of the ±1 and ±3 channels increase with height when the PWV amount is less than 2.5 mm. From comparison with National Weather Service (NWS) AIR VIZ RSs, [5] and [14] estimated that the error contribution due to RS uncertainties could be as high as 10 K or 20 K. A detailed discussion on the Vaisala RS92 humidity sensor and its sources of errors can be found in [15]. The nighttime accuracy of Vaisala RS92 measurements in the upper troposphere and stratosphere, expressed as an error percentage (in percent) in reference to a Cryogenic Frost Point Hygrometer readings, was estimated in the same study [15, Table 3] to be $-13\% \pm 14\%$.

To assess the effect of this uncertainty on the computed brightness temperature, we analyzed the only six soundings with a PWV of less than 2.5 mm (shown in Fig. 3). The profiles

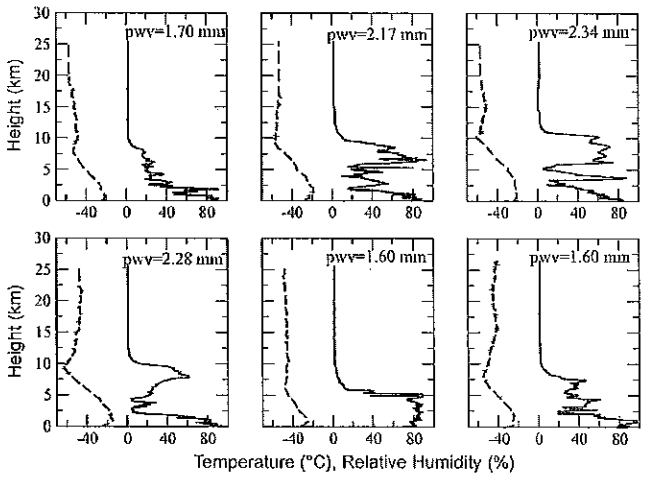

Fig. 3. Six RS soundings used to assess the effect of errors in the soundings above 10 km. The dashed line is the temperature profile (in degrees Celsius) and the solid line is the RH profile (in percent).

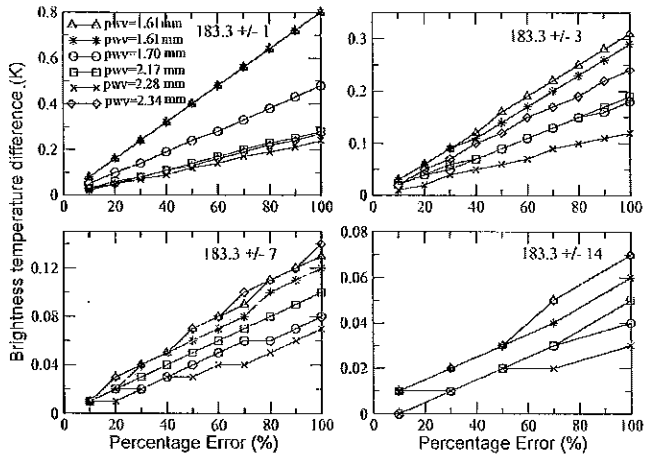

Fig. 4. Differences between brightness temperatures computed from modified and original soundings. In the modified soundings, the RH above 10 km was changed according to $\mathrm{RH}(i) = (1+\varepsilon)\mathrm{RH}_{\mathrm{orig}}(i)$ with $\varepsilon > 0$.

were extrapolated to 25.5 km and the brightness temperatures computed. The relative humidity (RH) in the layers above 10 km was then expressed as

$$\mathrm{RH}(i) = (1+\varepsilon)\mathrm{RH}_{\mathrm{orig}}(i) \tag{1}$$

where $\mathrm{RH}_{\mathrm{orig}}$ is the original RS profile and $0 \leq \varepsilon \leq 1$. Brightness temperatures were then computed for ten different values of ε. The differences between brightness temperatures computed from the modified ($\varepsilon > 0$) and original ($\varepsilon = 0$) profiles are shown in Fig. 4 for the four GVR frequencies. When $\varepsilon = 1$, the percentage error of the original measurement is 100% (the RH is doubled). In Fig. 4, the six profiles are shown individually to highlight the dependence on the PWV. The two profiles with a PWV of 1.6 mm show the strongest dependence on changes in the stratospheric water vapor as expected. In our simulation, even assuming an error of 100%, the difference in the simulated brightness temperatures is less than 1 K for the 183.3 ± 1-GHz channel when the PWV is 1.6 mm. For the same percentage error, the 183.3 ± 3-GHz channel has a maximum difference in brightness temperature of 0.3 K. The remaining two channels do not display a large sensitivity to upper layer errors, with differences of less than 0.1 K. Since PWV of less than 1.5 mm was not encountered during the time examined, the effect of stratospheric water vapor on even dryer profiles will be the subject of a more detailed subsequent study, when more soundings will be available. The effect of RS uncertainties in the lower troposphere will be studied as well. Since [5] and [14] reported brightness-temperature differences as high as 10 or 20 K associated with certain types of humidity sensors, we attempted to reproduce such results by arbitrarily setting the RH of all layers above 10 km to a value of 20% ($\varepsilon \sim 6$). This gives brightness-temperature differences as high as 8 K for a PWV of 1.6 mm consistent with the previously mentioned findings. NWS RSs have been found to be largely incorrect in their upper troposphere measurements by [16]. We estimate a percentage error of 600% for the RS92 RS to be unrealistic even in very dry conditions. In Table II, for each profile, we summarize the difference between modeled and measured brightness temperatures, the possible contribution due to errors in the layers above 10 km and estimated measurement errors based on the revised calibration described in the previous section.

V. Sensitivity to PWV and LWP

The sensitivity of the GVR channels to the presence of water vapor is much stronger than that of the 22-GHz water-vapor line [5]. In Fig. 5, the dependence of GVR-measured clear-sky brightness temperatures on PWV is shown. The PWV is retrieved from the MWR measurements. The circles, diamonds, triangles, and squares are model computations from one year of RS data. Fig. 5 shows the nonlinear response of the GVR to water vapor as well as the saturation of the channels close to the line center. These results are consistent with those of [5], which estimated the sensitivity to PWV at these frequencies to be approximately 30 times higher than at the frequencies of the MWR for PWV less than 2.5 mm. To assess the sensitivity to LWP, three months of RS data (clear and cloudy) were used to compute brightness temperatures. Because the RSs do not measure liquid water, differences between model and measurements were attributed to the presence of liquid-water clouds. Fig. 6 shows the difference between measured and modeled brightness temperatures as a function of LWP retrieved with the MWR. Because the uncertainty in MWR retrievals is about 20 g/m^2, data with LWP < 0.02 mm were considered clear. For comparison, the same difference is shown for brightness temperatures measured by the MWR. The ratio $\Delta\mathrm{Tb}/\Delta\mathrm{LWP}$, the slope of the linear fit, is an indication of the sensitivity to LWP. In Table III, the slope is displayed for the two MWR channels and for two of the GVR channels. The 183.31 ± 14-GHz channel has a sensitivity that is about 3.5 times greater than the 31.4-GHz channel of the MWR.

VI. Retrieval Algorithm

A nonlinear algorithm was used to retrieve LWP and PWV from GVR measurements. The algorithm is a Gauss–Newton

TABLE II
BRIGHTNESS-TEMPERATURE DIFFERENCES

Profile (yy/mm/dd)	PWV (mm)	Brightness temperature differences (K)				Notes
		183.3±1	183.3±3	183.3±7	183.3±14	
05/12/06	2.17	−5.74	−6.84	−1.60	−3.04	(1) Measurements–Model (ε=0)
		−0.14	−0.09	−0.05	−0.02	(2) Model (ε=0)–Model (ε=+50%)
		−0.28	−0.19	−0.10	−0.05	(3) Model (ε=0) –Model (ε=+100%)
		0.95	0.61	0.39	−0.02	(4) Recalibrated–Original Measurements
05/12/21	2.34	−3.06	−1.85	1.84	−1.06	
		−0.13	−0.12	−0.07	−0.03	
		−0.27	−0.24	−0.14	−0.07	
		1.03	0.72	0.44	0.007	
06/01/04	2.28	0.39	0.54	3.04	−0.76	
		−0.12	−0.06	−0.03	−0.02	
		−0.24	−0.12	−0.07	−0.07	
		1.02	0.76	0.50	0.044	
06/01/20	1.60	−6.58	−5.14	0.25	−1.24	
		−0.40	−0.16	−0.06	−0.03	
		−0.80	−0.31	−0.12	−0.06	
		0.67	0.37	0.28	-0.08	
06/01/26	1.60	−6.84	−5.93	−1.63	-2.45	
		−0.39	−0.14	−0.06	−0.03	
		−0.79	−0.29	−0.12	−0.06	
		0.66	0.36	0.26	−0.09	

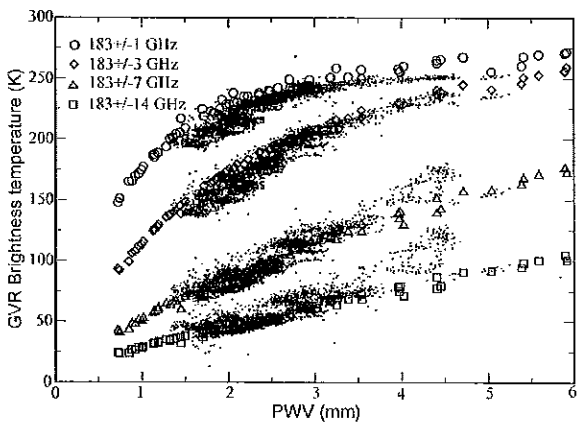

Fig. 5. GVR-measured brightness temperatures as a function of PWV retrieved from the colocated MWR. Data are for noncloudy conditions only. The circles, diamonds, triangles, and squares are model computations from one year of RS data. The nonlinear response to PWV is evident in the ±1 and ±3 channels.

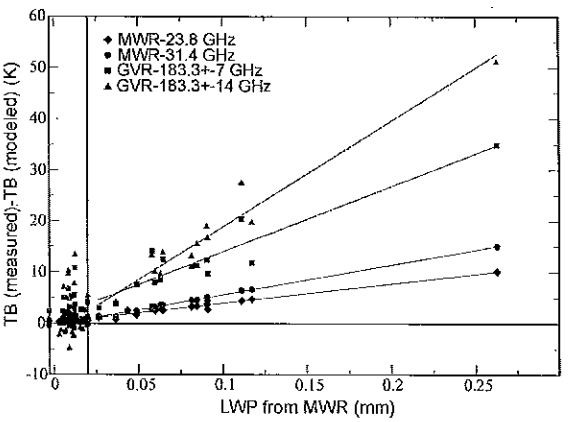

Fig. 6. Sensitivity of GVR-measured brightness temperatures to LWP. The LWP on the x axis is retrieved from the colocated MWR.

method [17] that finds the zeroes of the gradient of the cost function $\mathbf{J}$

$$\mathbf{J} = [\mathbf{y} - \mathbf{F}(\mathbf{x})]^{\mathrm{T}}\, \mathbf{E}^{-1}\, [\mathbf{y} - \mathbf{F}(\mathbf{x})] + [\mathbf{x} - \mathbf{x}_{\mathrm{a}}]^{\mathrm{T}}\, \mathbf{S}_{\mathrm{a}}^{-1}\, [\mathbf{x} - \mathbf{x}_{\mathrm{a}}] \tag{2}$$

where the superscript T indicates the transpose matrix. In (2), $\mathbf{x}$ is a 27-element vector whose first element is LWP and whose remaining 26 levels constitute an RH profile between 0 and 10 km. The *a priori* constraint $\mathbf{x}_{\mathrm{a}}$ is computed from one year of RS data with covariance $\mathbf{S}_{\mathrm{a}}$. The vector of computed brightness temperatures is $\mathbf{F}(\mathbf{x})$, and $\mathbf{y}$ is the vector of the GVR measurements with error covariance $\mathbf{E}$. The minimization is achieved by successive iterations starting from a first-guess profile of temperature and RH. The first-guess profiles are retrieved by linear statistical regression from measurements collected by the 12-channel Microwave Radiometer Profiler (MWRP) [18]. At each iteration, the contribution of stratospheric water vapor

TABLE III
SLOPE OF LINEAR-REGRESSION FIT

Frequency (GHz)	Slope ΔTb/ΔLWP (K/mm)
23.8	38.53
31.4	58.71
183.3 ± 7	130.39
183.3 ± 14	205.92

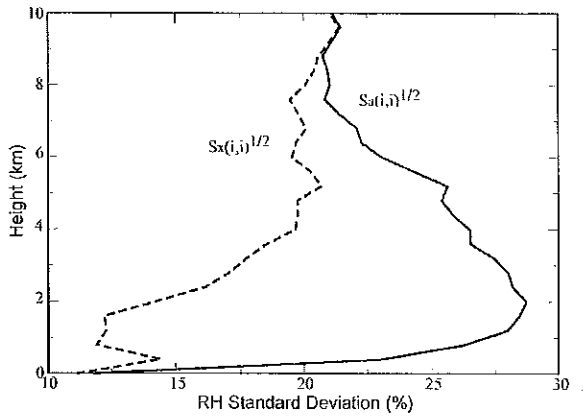

Fig. 7. Example of standard deviation for a retrieved RH profile. The solid line is the prior standard deviation. The postmeasurement covariance is the same as the prior in the region where measurements are not contributing to the retrieval.

was accounted for by adding a layer of constant temperature and humidity (3%) between 10 and 25 km. For the retrieval computations, we used a monochromatic approximation instead of the full-bandwidth integration. This will introduce a systematic error in the ±7- and ±14-GHz channels that have the largest bandwidth. Negative LWP are set to zero during the iteration process, however the constraint is relaxed on the last iteration. The criterion for convergence is that the difference between two successive estimations be smaller than a predetermined threshold: $x_{n+1}(1) - x_n(1) < 0.005$ mm and $x_{n+1}(i) - x_n(i) < 20\%$ for $i = 2, 27$. Upon convergence, the algorithm returns the estimated vector $\hat{\mathbf{x}}$ and its error covariance $\mathbf{S_x}$. The postmeasurement covariance matrix $\mathbf{S_x}$ is defined as

$$\mathbf{S_x} = \left(\mathbf{K^T E^{-1} K} + \mathbf{S_a^{-1}}\right)^{-1} \tag{3}$$

where K is the Jacobian $K_{ij} = \partial f_i(x)/\partial x_j|_{\mathbf{x=xn}}$. The matrix $\mathbf{S_x}$ is an indication of how well the retrieval performs with respect to the climatologic average used as statistical constraint. The square roots of its diagonal elements are the standard deviation of the retrieval error at each layer. In Fig. 7, an example of $\sqrt{S_x(i,i)}$ is shown with $\sqrt{S_a(i,i)}$, the prior standard deviation. In the region where the measurements are not contributing to the retrieval, the standard deviation tends to the *a priori* constraint. This is noticeable at the very top layer, where the information from the measurements is low, and the bottom layer that is the surface-sensor measurement. The postmeasurement standard deviation is smaller than the prior in the region where the measurements are contributing. Factors contributing to the total retrieval covariance are measurement noise, forward model errors, and errors due to the use of a low-resolution atmospheric profile. In addition, any error in the instrument calibration will appear as a bias in the final result. The retrieved relative-humidity vector is first converted to specific humidity and, then, integrated to obtain PWV. The retrieved PWV error covariance is estimated following [17], by applying a transformation h to $\mathbf{S_x}$:

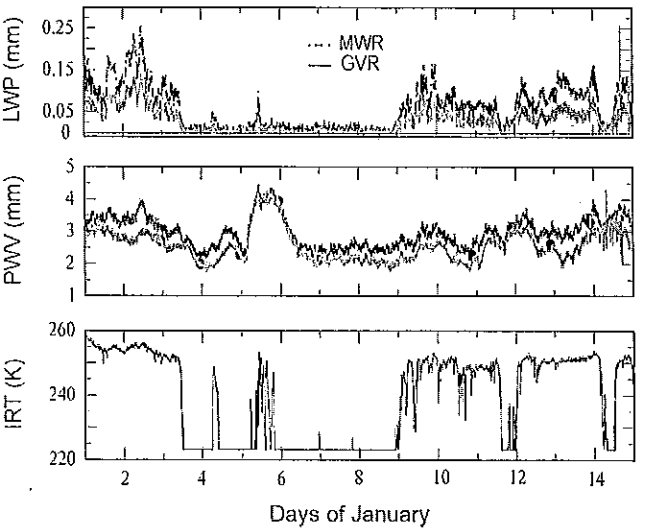

Fig. 8. Time series of PWV and LWP retrieved by the MWR and the GVR in January 2006. The MWR-retrieved parameters are slightly higher than the GVRs. The bottom panel is the infrared temperature measured by the 10-μm infrared thermometer located on top of the MWRP.

$$S_{\mathrm{PWV}} = \mathbf{h^T S_x h}. \tag{4}$$

In this case, h is the vector. $\overline{\mathbf{mr}}_{\mathbf{sat}}(\mathbf{T})\Delta\mathbf{p}$ necessary to convert RH to PWV, where $\overline{\mathbf{mr}}_{\mathbf{sat}}(\mathbf{T})$ is the layer average saturation mixing ratio (dependent on temperature T) and Δp is the layer pressure gradient. The standard deviation of the retrieval error is

$$\varepsilon_{\mathrm{PWV}} = \sqrt{s_{\mathrm{PWV}}} \tag{5}$$

$$\varepsilon_{\mathrm{LWP}} = \sqrt{S_x(1,1)}. \tag{6}$$

VII. RETRIEVAL RESULTS

A time series of retrieved PWV and LWP for January 2006 is shown in Fig. 8. Data were collected during prevailing low-humidity conditions. GVR retrievals have the same time resolution (5 min) as of the MWRP retrievals used to initialize the algorithm. The top panel is the retrieved LWP, while the middle panel is the retrieved PWV. In the bottom panel, infrared temperature measured by the Wintronics KT-19.85 infrared thermometer is shown. On the two top panels, the solid (gray) and dashed (black) lines are the GVR and MWR retrievals, respectively. The MWR retrievals are based on an *a priori* linear statistical retrieval trained with several years of *in situ* RS measurements. Gaussian noise with a standard deviation of 0.5 K is added in the retrieval to simulate a real instrument. The radiative transfer model MonoRTM is used in both retrievals. In the nonlinear physical algorithm for the GVR, a liquid-water

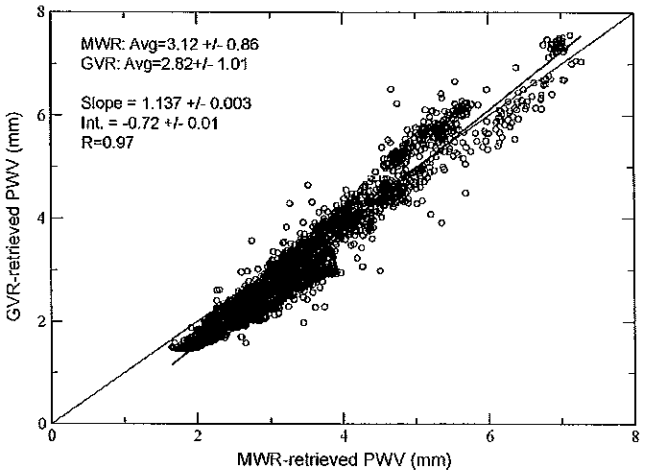

Fig. 9. Scatter plot of MWR-retrieved (x axis) and GVR-retrieved (y axis) PWV (data are from two weeks in December and January), $N = 6912$.

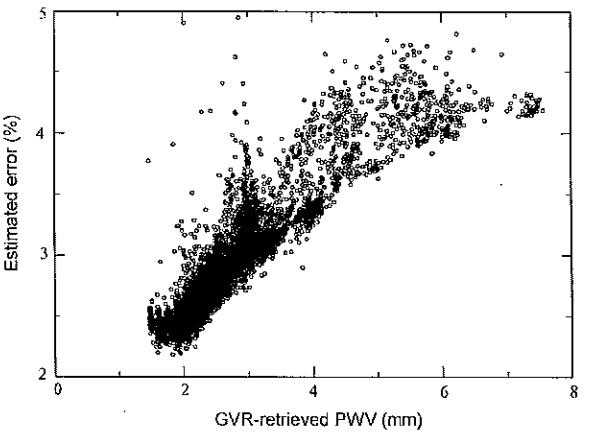

Fig. 10. Estimated error percentage of GVR-retrieved PWV as a function of PWV.

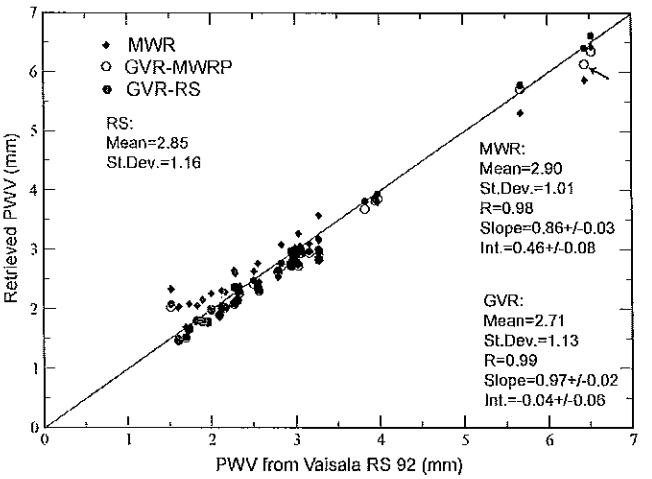

Fig. 11. Comparison of PWV retrieved from the MWR (diamonds) and the GVR (circles) with RS measurements during the months of November, December, and January ($N = 41$). The arrow indicates one case where the MWRP-retrieved temperature profile was largely incorrect (see text for details).

layer is inserted between 0 and 1 km. Computed brightness temperatures are independent of the location of the liquid layer, since the liquid-water-absorption model is not pressure dependent, although, it has a slight temperature dependence. Cimini *et al.* [19] show that liquid-water-weighting functions at these frequencies are constant in the first 5 km. The first noticeable feature of the comparison is that the GVR retrieves less LWP than the MWR. This is generally true during clear-sky conditions, as it will be shown later, however, it is also true under cloudy conditions. In the absence of additional LWP measurements, it is difficult to assess the accuracy of the LWP retrievals. The LWP retrieval error computed from (6) varies linearly between 0.004 and 0.012 mm as a function of PWV, while the difference between MWR-retrieved and GVR-retrieved LWP increases linearly with the LWP. Although previous studies have shown that MWR retrievals of liquid water may be too high at times, it is possible that the differences in the retrievals may be due to issues in the iterative retrievals used for the GVR. Additional investigation is needed to clarify this point, especially the role of the prior information and statistical constraints. It is also important to notice that we neglected the possible effect of scattering on the 183.3 ± 14-GHz channel. The sensitivity of this channel to ice scattering was estimated by [19] and found to be negligible (< 0.6 K) at the frequencies analyzed here for typical winter ice clouds. Since the presence of ice water path (IWP) will increase the brightness temperature observed by the 183.3 ± 14 GHz channel, the presence of IWP would be interpreted as a contribution from liquid clouds.

In Fig. 9, a scatter plot of MWR- and GVR-retrieved PWV is shown for cloudy and clear-sky cases during the two weeks in December 2005 and the two weeks in January 2006. When the PWV is very low (PWV < 4 mm), it appears that the GVR retrieves less PWV. The difference between the PWV averages (MWR − GVR) is 0.3 mm. Fig. 10 shows that the PWV error percentage, as estimated from (5), varies approximately between 2% and 4.5% for a range of retrieved PWV between 1.5 and 7.5 mm. Fig. 11 shows a comparison of retrieved PWV with measurements from Vaisala RS92 RSs during the months of November, December, and January. The expected accuracy of RH measurements for the Vaisala RS92 RS is estimated at about 5%. This translates to a PWV accuracy of less than 1 mm. The diamonds are MWR retrievals, while empty circles are GVR retrievals using the MWRP-retrieved profile to initialize the algorithm. For the cases shown in Fig. 11, the MWR slightly overestimated water vapor when RS measurements were below 3 mm. In contrast, GVR retrievals slightly underestimated (0.1 mm) PWV. In addition to the total retrieval error defined in (5) and shown in Fig. 10, we examined the influence of the first guess. We carried out the retrieval in proximity to RS launches and used the RS profiles, as the first guess, instead of the MWRP-retrieved profiles. Wang *et al.* [20] showed that an unrealistic first guess could influence the outcome of the water-vapor retrieval at these frequencies even if a stricter convergence criterion is imposed. The uncertainty in MWRP RH profiles is estimated to be about ±20%, however, it may exceed this value. The results of this exercise, shown in Fig. 11 as black filled circles, suggest that the uncertainty, related to the RH first guess, is not a large source of error. However, upon closer examination, it was found that uncertainties in the

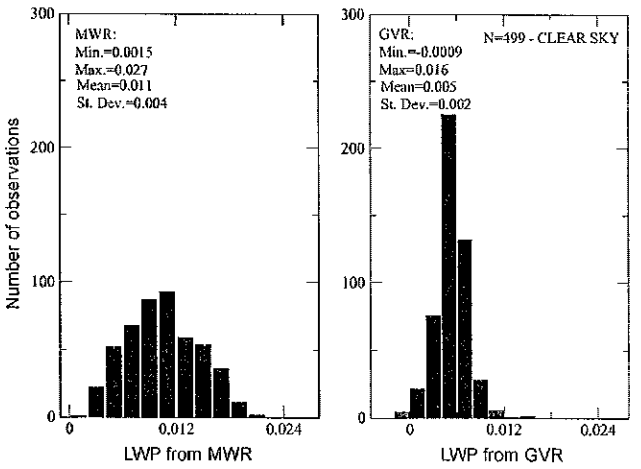

Fig. 12. Clear-sky LWP distributions retrieved by the MWR (left panel) and the GVR (right panel). $N = 499$ cases in January 2006.

temperature profile derived from MWRP measurements were responsible for some of the discrepancies in the retrieved PWV. For example, for the data point indicated by an arrow in Fig. 11, the MWRP-retrieved temperature profile overestimated the RS profile by about 5 K below 2 km and was underestimated it above 2 km, reaching a maximum difference of about 10 K at 9 km. When the retrieved temperature profile was used instead of the RS profile in the conversion from RH to PWV, the PWV decreased from 6.41 to 6.14 mm. The uncertainty in the temperature retrieval is more prominent during clear conditions, because the radiometer is not able to accurately reproduce pronounced low-level temperature inversions.

VIII. Clear-Sky LWP Retrievals

The analysis of LWP retrieval under clear-sky conditions is important to assess uncertainties that will affect LWP retrieval under cloudy conditions. In the absence of clouds, the LWP should be zero, however, because of uncertainties in the conversion from brightness temperature to physical quantities, the retrieved LWP will not be exactly zero. Uncertainties in the MWR clear-sky retrievals have been analyzed in [2] and [4] and have been attributed to modeling of the dry opacity term and to the cloud-liquid-absorption coefficient. This effect will lead to the retrieval of a positive amount of LWP even when the sky is clear. MWR-retrieved amounts during clear days can be as large as 20 g/m^2. At 183.31 GHz, the effect of uncertainties in the oxygen line modeling should be negligible; therefore, uncertainties related to this term should not affect the retrieval. Both MWR and GVR retrievals use the same liquid-water-absorption model of [21]. A distribution of retrieved clear-sky LWP from the two instruments is shown in Fig. 12 for January 6–8. On the left panel is the MWR retrieval, and on the right panel, is the GVR retrieval. Both retrievals display a positive bias. The positive bias ($\sim$0.013 $\pm$ 0.04 mm) in the MWR retrievals is partially due to the modeling of the dry opacity as mentioned earlier. GVR retrievals have less bias ($\sim$0.005 $\pm$ 0.002 mm). Results in Table II suggest that uncertainties in the assumption of water-vapor distribution above 10 km are not a significant source of error in the LWP retrieval; however, the monochromatic approximation will introduce an error in the modeled brightness temperatures at the two frequencies (183.3 $\pm$ 7 and $\pm$ 14 GHz) that are sensitive to liquid clouds. In addition, the model-measurement bias in the 183.3 $\pm$ 1- and $\pm$ 3-GHz channel (Table I) will contribute to the retrieval error. The observed differences between model and measurements could come from the modeling of the line absorption (most probably the line half-width parameter) and from uncertainties in brightness-temperature measurements. As mentioned in Section III, differences in the formulation of the water-vapor continuum were found to cause differences of 1–2 K in modeled brightness temperatures [4]. In addition, the value of the self-broadening parameter of the 183.3-GHz line from HITRAN is about 11% smaller than the value used in [4]. Uncertainties in the measurements can be caused by inaccurate measurements of the temperature of the reference loads. Although these could lead to errors of more the 2 K in the coldest channel, such errors were not detected when the calibration was verified using a more accurate calibrator, as described in Section II and shown in Table II for five cases.

IX. Conclusion

We have analyzed a set of measurements from a GVR during the Arctic winter. The instrument was designed to improve water-vapor and liquid-water retrievals needed in radiance simulations and climate models for very dry conditions. This is the first time such an extensive set of ground-based data has been available at these frequencies.

We have compared measurements with model computations and developed a retrieval algorithm for PWV and LWP. For the comparison with the model, we computed brightness temperatures using the full-channel bandwidth. Differences between measurements and model were 2%–3% for all channels. The largest discrepancies were found at frequencies close to the line center ($\pm$1 $\pm$ 3 GHz). Possible sources of error in the comparison are: model uncertainties; errors in RS soundings; and inaccurate calibration. Model uncertainties due to different water-vapor continuum and line parameters have not been examined in detail in this paper, however, from previous studies [4], [5] and additional simulations (not shown), they have been estimated to contribute $\sim$1–2 K to the model uncertainty. The errors associated with RS soundings above 10 km were examined by analyzing six representative cases with PWV of less than 2.5 mm. It was found that, in the range of PWV encountered during the period analyzed (PWV $>$ 1.6 mm), these errors have a magnitude of $\sim$0.8 K at the most. Errors in dryer (PWV $<$ 1.5 mm) conditions as well as errors due to uncertainties in the lower tropospheric soundings were not addressed in this paper and are left for a further study. Finally, calibration accuracy was estimated by comparing the original data (calibrated using a temperature sensor specified for a $\pm$0.2-K error) with a more accurate calibration load specified to have an accuracy of 0.05 K. The measured absolute error was less than 2 K in the four receiver channels over the brightness-temperature-measurement range. The revised calibration produced a slight increase in the brightness temperatures of the $\pm$1- and $\pm$3-GHz channel, slightly improving the agreement

with the model; however, the magnitude of the correction was ≤ 1 K at all frequencies.

A retrieval algorithm was developed for PWV and LWP, and results were compared with the colocated MWR retrievals and with RS measurements. The retrieval algorithm was implemented using a monochromatic approximation for all channels. While this approximation does not introduce a substantial error in the ± 1- and ± 3-GHz cannels ($\sim$0.5 K), it does have a noticeable effect (1–2 K) on the two remaining channels.

Retrievals using the GVR measurements generally produced lower values of LWP than did retrievals using the MWR measurements. GVR clear-sky LWP retrievals for two days in January have about half the mean and standard deviation of corresponding MWR retrievals. Retrieval errors under clear and cloudy conditions were estimated to vary between 0.004 and 0.012 mm, and the difference in the LWP retrieved by the two instruments increased at larger LWP amounts.

PWV retrieved from GVR measurements was compared with that retrieved from MWR measurements and computed from RS soundings. The GVR retrieved less PWV than the MWR when the PWV was less than $\sim$3 mm showing a better agreement with RS soundings. Retrieval errors have been estimated to be below 5% when the PWV is in the range of 1–8 mm. The MWRP-retrieved humidity profiles used as first guess (estimated error of $\pm 20\%$ RH) did not have a noticeable effect on the retrieval; however, MWRP-retrieved temperature profiles used in the conversion from RH to PWV were found to introduce errors of as much as 5% in the retrieval. This error is more pronounced during clear conditions when low-level temperature inversions are present and can be addressed by using more accurate temperature retrievals.

REFERENCES

[1] T. P. Ackerman and G. M. Stokes, "The Atmospheric Radiation Measurement program," *Phys. Today*, vol. 56, no. 1, pp. 38–44, Jan. 2003.

[2] R. Marchand *et al.*, "An assessment of microwave absorption models and retrievals of cloud liquid water using clear-sky data," *J. Geophys. Res.*, vol. 108, no. D24, 4773, Dec. 2003.

[3] S. Crewell and U. Löhnert, "Accuracy of cloud liquid water path from ground-based microwave radiometry 2. Sensor accuracy and synergy," *Radio Sci.*, vol. 38, no. 3, pp. 8042–8052, Feb. 2003.

[4] E. R. Westwater, Y. Han, M. D. Shupe, and S. Y. Matrosov, "Analysis of integrated cloud liquid and precipitable water vapor retrievals from microwave radiometers during the Heat Budget of the Arctic Ocean project," *J. Geophys. Res.*, vol. 106, no. D23, pp. 32 019–32 030, 2001.

[5] P. B. Racette *et al.*, "Measurements of low amounts of precipitable water vapor using ground-based millimeterwave radiometry," *J. Atmos. Ocean. Technol.*, vol. 22, no. 4, pp. 317–333, Apr. 2005.

[6] R. Lutz, T. T. Wilheit, J. R. Wang, and R. K. Kakar, "Retrieval of atmospheric water-vapor profiles using radiometric measurements at 183 and 90 GHz," *IEEE Trans. Geosci. Remote Sens.*, vol. 29, no. 4, pp. 602–609, Jul. 1991.

[7] J. R. Wang, P. Racette, M. E. Triesky, and W. Manning, "Retrievals of column water vapor using millimeter-wave radiometric measurements," *IEEE Trans. Geosci. Remote Sens.*, vol. 40, no. 6, pp. 1220–1229, Jun. 2002.

[8] A. Siegenthaler, O. Lezeaux, D. G. Feist, and N. Kampfer, "First water vapor measurements at 183 GHz from the high alpine station Jungfraujoch," *IEEE Trans. Geosci. Remote Sens.*, vol. 39, no. 9, pp. 2084–2086, Sep. 2001.

[9] E. R. Westwater *et al.*, "Microwave and millimeter wave forward modeling results from the 2004 North Slope of Alaska Arctic Winter Radiometric Experiment," in *Proc. 15th ARM Sci. Team Meeting*, Daytona Beach, FL, Mar. 14–18, 2005. [Online]. Available: http://www.arm.gov/publications/proceedings/conf15/extended_abs/westwater_er.pdf

[10] A. L. Pazmany, "A compact 183-GHz radiometer for water vapor and liquid water sensing," *IEEE Trans. Geosci. Remote Sens.*, vol. 45, no. 7, pp. 2202–2206, Jul. 2007.

[11] S. A. Clough, M. W. Shephard, E. J. Mlawer, J. S. Delamere, M. J. Iacono, K. Cady-Pereira, S. Boukabara, and P. D. Brown, "Atmospheric radiative transfer modeling: A summary of the AER codes, short communication," *J. Quant. Spectrosc. Radiat. Transf.*, vol. 91, pp. 233–244, 2005.

[12] L. S. Rothman *et al.*, "The HITRAN 2004 molecular spectroscopic database," *J. Quant. Spectrosc. Radiat. Transf.*, vol. 96, no. 2, pp. 139–204, Dec. 2005.

[13] S. A. Clough, F. X. Kneizys, and R. W. Davies, "Line shape and the water vapor continuum," *Atmos. Res.*, vol. 23, no. 3/4, pp. 229–241, Oct. 1989.

[14] J. R. Wang *et al.*, "Simultaneous measurements of atmospheric water vapor with MIR, Raman lidar and rawindsondes," *IEEE Trans. Geosci. Remote Sens.*, vol. 34, no. 7, pp. 1595–1607, 1995.

[15] L. M. Miloshevic, H. Vömel, D. N. Whiteman, B. M. Lesht, F. J. Schmidlin, and F. Russo, "Absolute accuracy of water vapor measurements for six operational radiosonde types launched during AWEX-G and implications for AIRS validation," *J. Geophys. Res.*, vol. 111, no. D9, D09S10, 2006. DOI: 10.1029/2005JD006083.

[16] V. Mattioli *et al.*, "Analysis of radiosonde and ground-based remotely sensed PWV data from the 2004 North Slope of Alaska Arctic Winter Radiometric Experiment," *J. Atmos. Ocean. Technol.*, vol. 24, no. 3, pp. 415–431, 2007.

[17] C. D. Rodgers, *Inverse Methods for Atmospheric Sounding. Theory and Practice*. Hackensack, NJ: World Scientific, 2000, p. 73.

[18] J. C. Liljegren, M. P. Cadeddu, and A. Pazmany, "Retrievals of atmospheric temperature and water vapor profiles in the Arctic," in *Proc. 9th Specialist Meeting Microw. and Remote Sens. Appl.*, San Juan, Puerto Rico, Feb. 28–Mar. 8, 2006, pp. 241–246.

[19] D. Cimini, E. R. Westwater, A. J. Gasiewski, M. Klein, V. Leuski, and J. Liljegren, "Ground-based millimeter- and submillimeter-wave observations of low vapor and liquid water contents," *IEEE Trans. Geosci. Remote Sens.*, vol. 45, no. 7, pp. 2169–2180, Jul. 2007.

[20] J. R. Wang, P. Racette, and L. A. Chang, "MIR measurements of atmospheric water vapor profiles," *IEEE Trans. Geosci. Remote Sens.*, vol. 35, no. 2, pp. 212–223, Mar. 1997.

[21] H. J. Liebe, G. A. Hufford, and T. Manabe, "A model for the complex permittivity of water at frequencies below 1 THz," *Int. J. Infrared Millim. Waves*, vol. 12, no. 7, pp. 659–675, Jul. 1991.

Maria P. Cadeddu received the M.S. degree in physics from the University of Cagliari, Cagliari, Italy, in 1994 and the Ph.D. degree in physics from Heriot-Watt University, Edinburgh, U.K., in 2002.

She is currently the Instrument Mentor for the U.S. Department of Energy Atmospheric Radiation Measurement (ARM) program microwave instrumentation.

Dr. Cadeddu is a member of the American Geophysical Union.

James C. Liljegren received the B.S., M.S., and Ph.D. degrees in mechanical engineering from the University of Illinois, Urbana, IL, in 1980, 1983, and 1989, respectively. His dissertation focused on the stochastic modeling of turbulent dispersion in the convective boundary layer.

In 1990, he joined the Pacific Northwest National Laboratory, where he became involved in ground-based microwave radiometry with the U.S. Department of Energy Atmospheric Radiation Measurement (ARM) Program. He joined the Ames Laboratory, Ames, IA, in 1997, where he continued to pursue research related to microwave radiometry and retrieval algorithm development. Since 1999, he has been with the Argonne National Laboratory, Argonne, IL, where he became the Site Program Manager for the ARM Southern Great Plains Climate Research Facilities in Oklahoma and Kansas in 2000 and has been the ARM Instrument Team Coordinator since 2003.

Dr. Liljegren is a member of the American Meteorological Society and the American Geophysical Union.

Andrew L. Pazmany (S'90–M'93) received the B.S., M.S., and Ph.D. degrees in electrical engineering from the University of Massachusetts, Amherst, MA, in 1986, 1988, and 1993, respectively.

He is currently a Senior Engineer at ProSensing Inc., Amherst, developing custom radar and radiometer systems for environmental remote sensing applications.